AIAA Scitech 2019 Forum, 7-11 January, San Diego, CA, USA
DOI:10.2514/6.2019-0265

Non-elliptic lift distribution wings to decrease vertical tailplane size in commercial aircraft

Martin Carrizalez[a], Estela Bragado[b] and Mudassir Lone[c]
Aerospace Integration Research Centre, Cranfield University, Cranfield, UK, MK43 0AL

Aircraft performance can be assessed and improved by considering the key variables linked to weight and aerodynamics in the Breguet range equation. In this paper, the authors present a method for wing design that allows a reduction in induced drag and minimization of the weight associated with the aircraft's vertical tailplane, whilst ensuring desirable lateral-directional flight dynamics. The use case is a general aviation aircraft for which the wing has been modified using Prandtl's 1933 approach where the span constraint is removed to yield a non-elliptic lift distribution. It is shown that such a lift distribution also contributes to the aircraft's lateral-directional stability and as a result, the size and weight of the vertical tail can be reduced. This study was carried out using an analytical framework that combines early design tools such as XFOIL and AVL deemed to be adequate for subsonic flight. Both cruise and approach configurations are considered. Wing twist distribution and span extension have been calculated using lifting line theory. The study demonstrates the design trade-off needed between flight dynamic modes, such as the Dutch roll mode, and vertical tailplane size when the aircraft is equipped with a wing designed to generate a non-elliptic lift distribution. It is shown that this approach allows a 14% improvement in the lift to drag ratio with 44.34% reduction in V-tail weight. These yield a total of 17% improvement in aircraft range. As for the approach phase it share all the characteristics observed in cruise with the difference that Dutch roll mode is stable for almost all the smaller size of V-tail. Further work requires to focus on the placement of ailerons to remove adverse yaw tendencies.

I. Introduction

Currently, aircraft manufacturers are looking into new ways of increasing aircraft efficiency and the focus on reducing airframe weight has been a major design driver along with aerodynamic performance. These two design drivers are often treated independently where structural engineers have focused on extending the use of lightweight advanced materials and aerodynamics engineers have focused on overall aircraft geometry. Aircraft such as the Boeing 747 and the Airbus A-320 have weight distributions over the airframe components as shown in Table 1.

Component/Aircraft	B727		ATR-42		A320-200		B747-100	
Wing	8401	33.72%	1760	30.40%	8801	39.99%	40160	41.71%
Horizontal tail	875	3.51%	220	3.80%	625	2.84%	3629	3.77%
Vertical tail	1007	4.04%	322	5.56%	463	2.10%	1786	1.86%
Fuselage	10152	40.75%	2587	44.69%	8938	40.61%	32062	33.30%
Main Landing Gear	2957	11.87%	534	9.22%	2275	10.34%	12458	12.94%
Nose Landing Gear	517	2.08%					1442	1.50%
Nacelles	1007	4.04%	366	6.32%	907	4.12%	4737	4.92%
Total	24916		5789		22009		96274	

Table 1 Weight breakdown for difference transport aircraft [1]

Table 1 shows that the Vertical Tail plane (VTP) weight can contribute anywhere between 2% to 6% of the total weight. The reason for this is to provide sufficient trim in the event of a engine failure for multi-engine

[a] Research Student, Centre for Aeronautics, School of Aerospace, Transport & Manufacturing.
[b] Research Student , Centre for Aeronautics, School of Aerospace, Transport & Manufacturing.
[c] Senior Lecturer, Centre for Aeronautics, School of Aerospace, Transport & Manufacturing.

aircraft, restore the aircraft from a upset yaw and adequate control power in critical conditions like engine-out at low speed, maximum roll rate and spin recovery[4]. For novel aircraft designs currently being researched, the position of the power plants is shifted from below the wings to the empennage area near the aircraft center line to exploit technologies such as boundary layer ingestion. Some examples are configurations such as the Airbus 2050 concept plane, e-Thrust concept and D8 that are shown in Figure 1(a).

(a) Airbus 2050 concept plane (b) e-Thrust concept (c) D8

Figure 1 Transport aircraft concepts with engines near center line

These types of aircraft have the advantage that in an engine-out scenario the requirement to generate large compensatory yawing moments may no longer be required. For such configurations the primary driver when sizing the VTP is the need for coordinated turn or put in other words, the need to compensate for adverse yaw characteristics. Past studies like the one performed by Van Dam et al[5] demonstrated the effectiveness of winglets in reducing the adverse yaw effect through wind tunnel tests. However, the introduction of winglets results in added weight and winglets are effectively a subset of solutions to reduce induced drag via span extension. Moreover, winglets are a means by which the designer achieves Oswald efficiency (e) factor above 1 by modifying the spanwise wing lift distribution. However, in this study the authors investigate an alternative way to reduce the airframe weight by maximising the efficiency of the primary aircraft component (the wing) both in terms of aerodynamics and its contribution to the aircraft's flight dynamic characteristics by using a non-elliptic lift distributions wing [6] that can provide proverse yaw characteristics[7] in order to minimise the VTP size.

In this study, the authors look into a way to reduce the weight of the aircraft by modifying the wing using an approach proposed by Prandtl in 1933 which advocated the use of a non-elliptic lift distribution combined with span extension to give improved performance. Moreover, such a distribution has also been found suitable for addressing the adverse yaw characteristics seen on flying wings. Here, the authors carry out a parameter variation study where the size of the vertical tailplane is reduced systematically for a general aviation aircraft to reduce its airframe weight and thus improve its range. This paper is structured such that the reader is given a brief overview of non-elliptical lift distributions wings in Section **II**. Section **III** present the readers to the in-house tool develop to perform the analysis by the use of low fidelity aerodynamic models. In Section **IV** the planform and flight conditions are presented as well the cases to be analysed. Section **V** focuses on the comparison and discussion of the results obtained. Finally, Section **VI** presents the key conclusions of the study and listing areas of further work.

II. Non-elliptic lift distribution wings

The Lifting Line Theory has remained the standard tool for the conceptual analysis of three-dimensional wings and the derivation of lift and induced drag. It is well known that the solution to this theory for wings with minimum induced drag with a given span are given by the elliptic spanwise loading. Nevertheless, in 1933 Prandtl publishes an alternative solution[6] in which he presents a superior spanload distribution, where the span is allowed to vary and the lift and local bending moment of the lift distribution are given instead. This assumption provides bell-shaped curve solutions that yield minimum induced drag for a given structural weight. The induced drag becomes determined by the lift and its moment of inertia, derived from the given integrated bending moment. Using this methodology, Prandtl showed the existence of solutions that provided an 11% induced drag reduction with a 22% span increase when compared to an equivalent wing with an elliptic distribution.

The application of non-linear spanwise twist allows the creation of such a spanload distribution, which yields a smooth upwash outboard of the wing, shifting the vortex inboard of the semi-span. In this region,

local negative induced drag is created, consequently reducing the total induced drag. Altogether, this gave the possibility to address adverse yaw by achieving a coordinated turn without the use of a vertical tailplane.

In this paper, both methodologies have been combined to achieve an analytical solution for the required twist distribution, which will provide Prandtl's optimal bell-shaped spanloads. The fundamental lifting-line integro-differential equation is shown in Equation1, generalised to account for camber effects and wing twist.

$$\frac{-2\Gamma(y)}{C_{l_\alpha}(y)\, c(y)\, V} - \frac{1}{4\pi V}\int_{-b/2}^{b/2} \frac{\frac{d\Gamma(y_0)}{dy} dy_0}{y - y_0} - \alpha_{0_c}(y) + \alpha_{0_t}(y) = 0 \tag{1}$$

This equation is a decomposition of the local angles of attack at each spanwise station, showing it as a summation of the effective, induced, camber and twist angles respectively. Thus, if the flight conditions and the circulation distribution are known, it is simple to extract the $\alpha_{0_t}(y)$ necessary to yield the desired spanload. In this case, the non-elliptic circulation distribution for minimum drag presented by Prandtl is used as a design constraint, shown in Equation 2:

$$\Gamma(y) = \Gamma_0 \left(1 - \mu \left(\frac{y}{b_P/2}\right)^2\right) \sqrt{1 - \left(\frac{y}{b_P/2}\right)^2} \tag{2}$$

where the solution for minimum D_i lies at $\mu = 1$, describing a bell-shaped curve instead of an elliptic one. In his paper, Prandtl also presents the solutions for the circulation at the root Γ_0 and the induced downwash $w_i(y)$, assumed as a second order polynomial. With this, and combining Equation 1 and 2 it is possible now to determine the analytical solution for the twist, which becomes:

$$\alpha_{0_t}(y) = \alpha_{0_c}(y) - \frac{8}{\pi}\frac{1}{b^2}\frac{L}{V^2\,\rho}\left(\left(\frac{y}{b/2}\right)^2 - \frac{1}{2}\right) + \frac{32}{3\pi}\frac{1}{b\, c(y)}\frac{L}{V^2\,\rho\, C_{l_\alpha}(y)}\left(1 - \left(\frac{y}{b/2}\right)^2\right)^{\frac{3}{2}} \tag{3}$$

III. Review of aerodynamics analysis Framework

An in-house tool known as CONNIE (aerodynamiCs mOrphing aNalysis aNd aIrfoil intErpolation) was used to carry out the analysis and comparison of the baseline wing (with elliptic loading) with that of a wing with a *non-elliptic lift distribution*, and furthermore to perform a study investigating the effects of decreasing the size of the VTP. This tool is combines reduced order panel and vortex-lattice methods to allow rapid assessment of aerodynamic and flight dynamics. The framework is composed of three major subroutines that are **ALINA** (Airfoils LinerAr INterpolAtion), **RAISA** (Reduced AerodynamIcS Analysis) and **ROSARIO** (Reduced mOrphing Systems AeRodynamIc Optimizer). These subroutines can work independently or interact with each other as required and the overall framework architecture is shown in Figure 2.

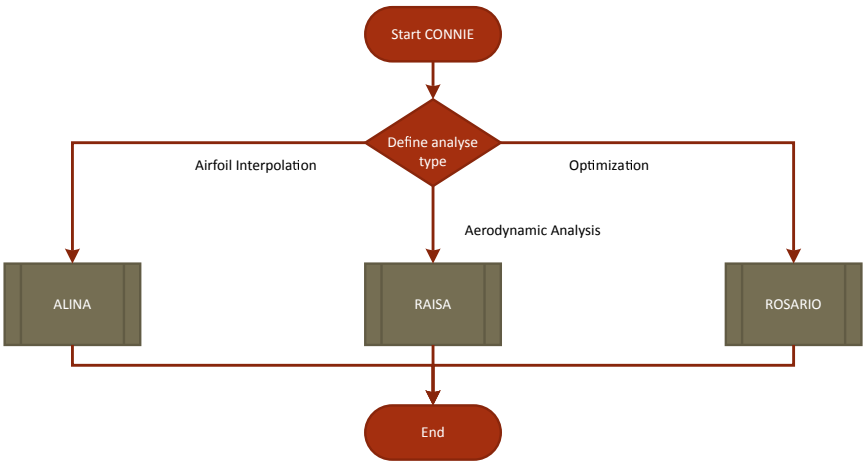

Figure 2 CONNIE framework diagram

In this study only the RAISA subroutine is used which performns the aerodynamics and flight dynamics analysis. RAISA works by employing *XFOIL* for 2D analysis. This is a low-order panel code which

implements a fully-coupled viscous/inviscid interaction model and it was developed from the work of Drela and Giles[8]. RAISA combines this with the 3D analysis resulting from *AVL* which is a vortex-lattice method (VLM) developed by Youngren that incorporates the work of Lamar[9], E. Lan and L. Miranda[10] among others. RAISA is therefore, capable of performing three types of analysis. It can perform 2D analysis on aerofoil sections for different values of velocities (v), altitudes (a) and angles of attack (α). The sectional aerodynamic forces are obtained by two different methods which use: (1) the direct surface pressures for C_L and C_M estimation and, (2) the Squire-Young formulation for estimating C_D. Starting with C_L and C_M, these are obtained by:

$$CL = \int C_p dx \quad C_M = \int -C_p \left[\left(x - x_{ref} d\right) dx + \left(y - y_{ref} d\right) dy \right] \tag{4}$$

where

$$x = x\cos(\alpha) + y\sin(\alpha) \tag{5}$$
$$y = y\cos(\alpha) - x\sin(\alpha) \tag{6}$$

as for C_p this is obtained by the use of the Karman-Tsien compressibility[11]:

$$C_p = \frac{C_{p_0}}{\sqrt{1-M^2} + \left[\frac{M^2}{1+\sqrt{1-M^2}}\right]\frac{C_{p_0}}{2}} \tag{7}$$

Here, M is the Mach number and C_{p_0} is the incompressible pressure coefficient over the aerofoil. As for estimating C_D, this is done by solving the Squire-Young formulation in the last point of the wake as follows:

$$C_D = \frac{D}{q} = 2\theta_i = 2\theta\left(\frac{u}{V}\right)^{\frac{H+5}{2}} \tag{8}$$

where θ represent the momentum thickness, u the edge velocity at the end of the wake, H the shape parameter and θ_i being the momentum thickness at the downstream infinity. As for the components of C_D they are given by:

$$C_D = C_{D_p} + C_{D_f} \tag{9}$$

Xfoil defines C_{D_p} and C_{D_f} as follows:

$$C_{D_p} = \int C_f dx \tag{10}$$
$$C_{D_f} = C_D - C_{D_p} \tag{11}$$

where C_f is the skin friction coefficient defined with the free stream dynamic pressure.

The use of AVL leads to certain limitations in the 3D analysis. First of all, sicne the flow is treated as quasi-steady, the results are only valid for small angles of attack (α) and sideslip (β). As for the compressibility effects, these are treated using the simple Prandtl-Glauert correction given by:

$$\gamma = \frac{1}{\sqrt{1-M^2}} \tag{12}$$

The panel forces are calculated using the Kutta-Joukowsky relation[12] applied to each vortex and when applied with the Prandtl-Glauert correction, it implies valid results up to $M = 0.6$ (subsonic limit) for unswept wings. Moreover, this approach for estimating the aerodynamic forces and moments does not allow the prediction of the viscous drag ($C_{D_{vis}}$) component. However, the strength of this approach lies in the fact that relatively accurate induced drag estimates can be obtained.

RAISA combines the aforementioned tools by taking the 2D $C_{D_{vis}}$ component of drag and applying it to the results of the 3D analysis. In order to do so, XFOIL analyses the aerofoil in each aerodynamic station or strip for the local Re, twist angle and α. This is done in order to obtain the C_{D_f} at each strip. Once XFOIL is finished, a normal 3D analysis is performed and the C_{D_f} values are introduced into the results at the corresponding strip position and the results are recalculated. This process is presented in Figure 3.

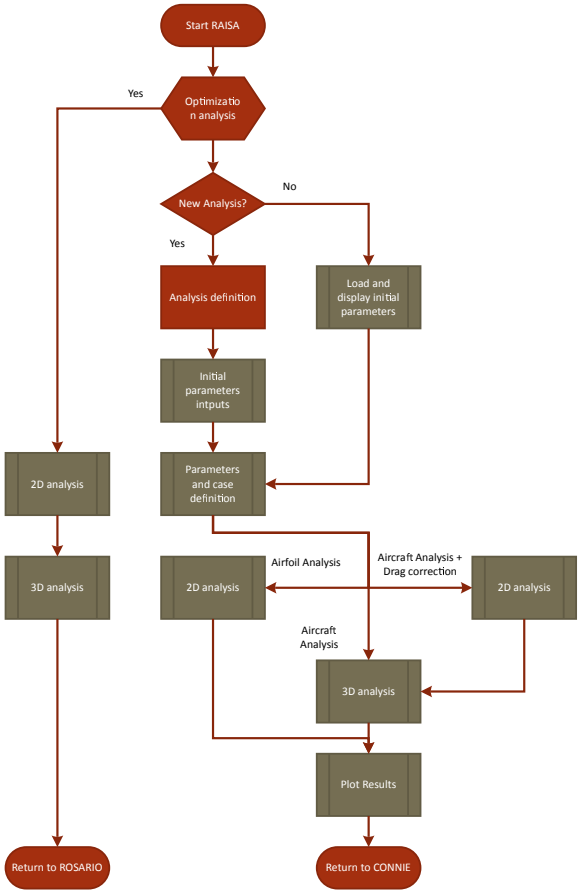

Figure 3 RAISA framework basic diagram

IV. Geometry and Case definition

Looking into smaller size transport aircraft, currently there are only two aircraft that have the powerplant along their center lines. These are the Cirrus SF50[13] and the Flaris LAR01[14]. The latter aircraft is undergoing testing and certification whilst the Cirrus SF50 is in full operation. Hence, the authors selected the Cirrus SF50 purely because of the information available in the public domain. Figure 4 and Table 2 present the main specifications for this aircraft.

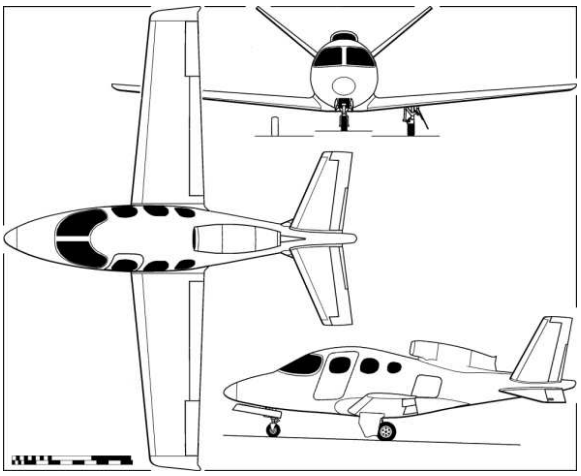

Figure 4 SF50 aircraft

Specification	Values
Wing Area (m^2)	18.08
Wingspan (m)	11.67
Root chord (m)	1.88
Taper ratio (λ)	0.648
Sweep angle (Λ)	5.65 $^\circ$
Dihedral angle (Γ)	5.83 $^\circ$
Length (m)	9.36
Max T-O (kg)	2722
Service celling (m)	8535
Max level Mach	0.53

Table 2 SF50 characteristics

Further to having a single engine along its centreline, this aircraft has the particularity of having a V-tail. This introduces the need for clear definitions for vertical and hirizontal tail volume coefficients. This addressed by adopting the work done by Purser and Campbell[15] who introduce the following relationship for V-tail configurations:

$$S_{V_{Tail}} = S_H + S_V \tag{13}$$

where S_H is the equivalent horizontal surface and S_V is the equivalent vertical surface. Since the specifications of the V-Tail are not available some inverse engineering was done by using Figure 1(a) and a CAD software. Table 3 presents the characteristics of the projected Horizontal tail plane (HTP) planform.

Specification	Values
Area (m^2) (S_{HTP_p})	5.07
Span (m)	4.43
Root chord (m)	1.53
Taper ratio (λ_p)	0.50
Sweep angle (Λ_p)	23.94 °
Dihedral angle (Γ_p)	38.55 °
Arm length (m) (L_H)	4.29

Table 3 Projected HTP specifications

The S_{HTP_p} parameter can be also obtained from the following:

$$S_{HTP_p} = S_{V_{Tail}} \cos(\lambda_p) \tag{14}$$

and if the tails are assumed to meet at the centreline then:

$$\lambda_p = \tan^{-1}\left(\frac{S_V}{S_H}\right) \tag{15}$$

Then using Equations 13,14 and 15 it is possible to obtain the the values of S_H and S_V, that in this case are equal to $3.62m^2$ and $2.89m^2$.

Since the aim of this study is investigate the effects of varying VTP size, the next step is to create a test matrix with the configurations that need to be evaluated. Equation 16 presents how the parameter S_V is initially calculated:

$$S_V = \frac{V_v b_w S_w}{L_V} \tag{16}$$

where V_v is the vertical volume coefficient and for this aircraft it is equal to 0.058 (close to the typical values of 0.04 suggested by Raymer[4]). Details of the parameter variation study are presented in Table 4. The values range from 0.1 (that is the V_v require for a Jet transport aircraft) to 0.02 (values typically associated with sailplanes)[4].

V_v	S_V (m^2)	$S_{V_{tail}}$ (m^2)	ΔV_v	ΔW_{VTP}
0.1	4.919	8.546	0.70	31.15
0.089	4.412	8.039	0.53	23.36
0.079	3.904	7.531	0.35	15.57
0.069	3.397	7.024	0.18	7.79
0.058	2.889	6.516	0	0
0.048	2.382	6.009	-0.18	-7.79
0.038	1.874	5.501	-0.35	-15.57
0.027	1.367	4.994	-0.53	-23.36
0.017	0.859	4.486	-0.70	-31.15
0.007	0.352	3.979	-0.88	-38.94
0	0	3.626	-1.0	-44.35

Table 4 V_v cases, W and $S_{V_{tail}}$ contribution

The following three wing designs are used to illustrate the implications of reducing VTP size and using the characteristics of wings with non-elliptic lift distributions:

Baseline: Original wing used in the SF50.

Model 1: Baseline wing with modified twist and span extension as discussed in Section II.

Model 2: Baseline wing with only a twist distribution described in Equation 3.

Model 1 has a 22% span extension as shown in Figure 5(a), and a twist distribution shown in Figure 5(b), according to the theory discussed in Section II. Model 2 is included in this study in order to study the effects of purely adding the twist distribution to a wing with an elliptic lift distribution. This twist distribution is presented in Figure 5(b).

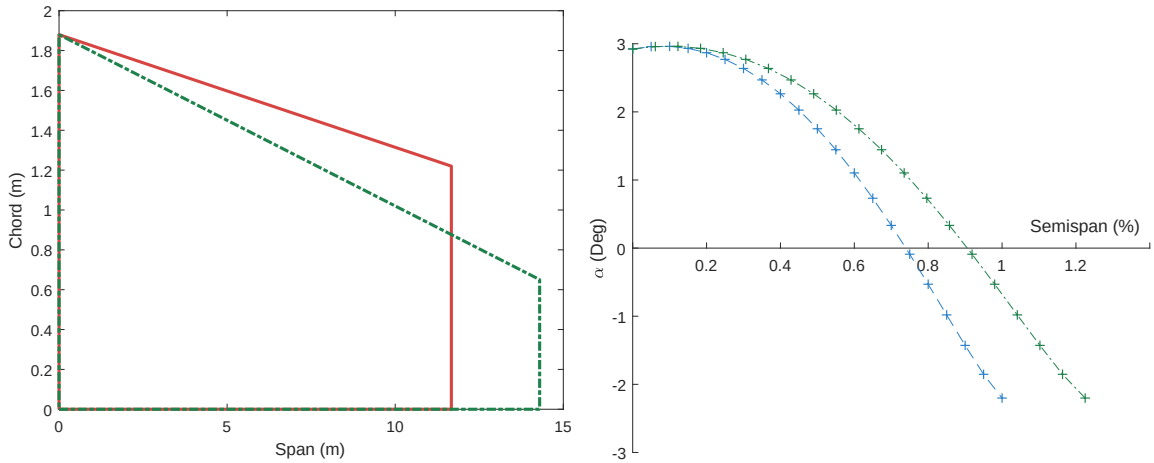

(a) Wing planform comparison

(b) Twist distribution comparison

Figure 5 Base ——, Model 1 -·-·-·-, Model 2 - - - -

In this study the authors have considered aircraft performance and flight dynamic characteristics for two flight conditions. The first is *Cruise* where the aerodynamic performance is critical. The second flight condition is *approach*, where the aircraft's flight dynamic characteristics are more important. As a result the assessment of flight dynamic stability and the analysis of the aerodynamic derivatives is only performed for approach conditions. Table 5 presents details of the two flight conditions.

Specification	Cruise	Approach
Altitude (m/ft)	8535/28000	91.44/300
Speed (m/s)	161.96	123.46
Mach	0.53	0.36
Reynolds number	$8.33x10^6$	$1.32x10^7$
α range	-5° to 11°	

Table 5 Cruise and Approach analysis conditions

V. Results and Discussion

A. Cruise condition

In order to assess the effects of adding a twist distribution to the wing (Model 2) and employing a non-elliptical wing (Model 1) a polar analysis was performed and then compared against the base configuration as shown in Figure 6(a). From this analysis the it can be seen that Model 1 gives an increase in L/D that can be translated to a 14% increase in Range (ΔR) while flying at 2 deg angle of attack. This is obtained by applying the Breguet range equation within which the range increase can be attributed to the increase in cruise C_L while maintaining a similar drag profile to the baseline wing. As for Model 2 a decrease in performance was observed, the decrease in the maximum L/D point results in a loss in R of 4% and this is primarily due to the increase in C_D.

The analysis for assessing the change in V-tail size can be carried out now that the L/D characteristics are known for each design. Eleven cases per wing design are considered for this analysis where a value of $-1$for ΔV represents the aircraft configuration without any vertical tailplane volume coefficient (V_v) contribution and

a value of 0.7 represents the maximum V_v contribution. The results of this comparison are shown in Figure 6(b) and the main observations are as follows:

- As expected, the increase in V_v results in a drop in ΔR drops (and vice-versa) for all the wing types due to the added VTP weight.
- Model 2 shows a decrease in ΔR for all cases that vary from 2% to 10% compared to the baseline case.
- The best V_v case in Model 2 has a decrease in ΔR of 0.5% against the worst case of the baseline wing.
- All Model 1 cases present an increase in ΔR that vary from 7% to 17%.
- A comparison of the worst case in Model 1 with the best case for the baseline wing shows an increase in R of almost 2%.

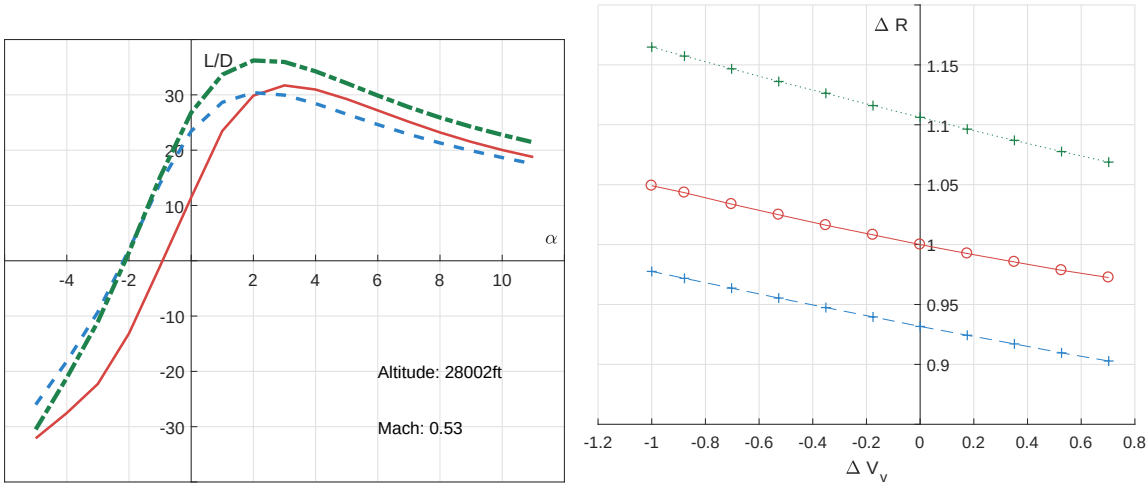

(a) Aerodynamic efficiency for a range of α

(b) Range analysis by wing type and ΔV_v coefficient

Figure 6 Base ——, Model 1 -·-·-, Model 2 - - -

Given that the aircraft with a non-elliptic lift distribution is shown to be more efficient, the next step is to observe if these configurations are stable from a flight dynamic perspective. From the results presented in Figure 7(a) it is possible to see that the short period and phugoid modes for all ΔV_v cases for each wing design are stable. The lateral-directional stability characteristics are presented in Figure 7(b). The roll subsidence and spiral modes in all cases are found to be stable. However, it can be seen that the Dutch-Roll mode tends towards the right half plane for all designs and in some cases is unstable as ΔV_v deceases. Therefore, it can be concluded that: (1) the baseline wing is stable only for values where $\delta V_v \geq 0$ and anything smaller will result in an unstable Dutch-Roll mode and, (2) for both Model 1 and Model 2 cases the aircraft will not show any Dutch-Roll instability if $\Delta V_v > 0$.

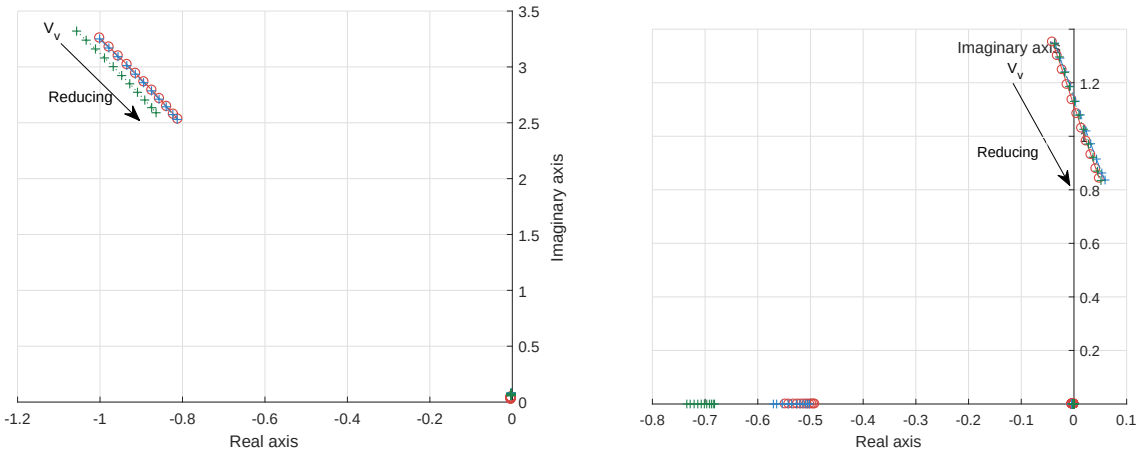

(a) Longitudinal stability root locus

(b) Lateral stability root locus

Figure 7 Base ——, Model 1 -·-·-·-, Model 2 - - - -

The flight dynamic characteristics of the aircraft can be studied in further detail by inspecting the key aerodynamic derivatives affected by the variation in VTP size, change in wing twist and the extension wing span. The first derivative to consider is the C_{m_α} which effectively indicates longitudinal static stability. This is driven by wing characteristics and can be approximated as:

$$\frac{dC_m}{d\alpha} = -C_{L_\alpha} K_n \tag{17}$$

where K_n is the static margin given by:

$$K_n = \bar{X}_{np} - \bar{X}_{cg} \tag{18}$$

where $\bar{X}_{np}$ the neutral point and $\bar{X}_{cg}$ the position of the center of gravity along the *X-axis*. The vairation of C_{m_α} with respect to VTP size is shown in Figure 8. It can be seen that Model 1 exhibits values of C_{m_α} which are larger in magnitude for all cases when compared to both the baseline and Model 2 cases. This can be attributed to the nature of the non-elliptic lift distribution which results in higher inboard loading and hence larger overall aircraft C_{L_α}. All cases for Model 2 result in the same C_{m_α} as the baseline design due to minimal change in wing planfrom and it can be seen that adding the twist alone has no real impact.

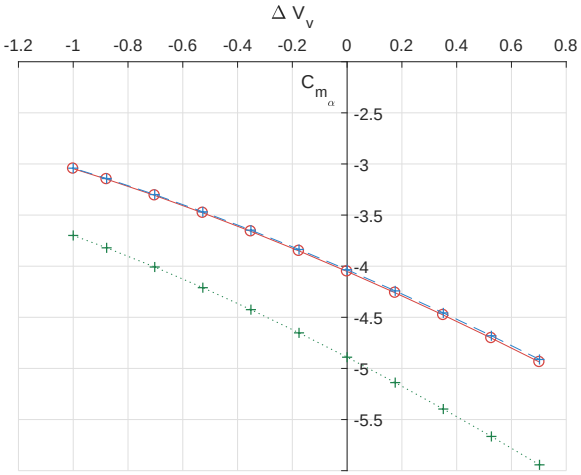

(a) Base ——, Model 1 -·-·-·-, Model 2 - - - -

Figure 8 Pitching moment due to normal velocity C_{m_α}

As for the lateral-directional derivatives which are significantly effected by the size of the VTP (since the VTP is used to counteract sideslip) one of the most important is *Rolling moment due to sideslip* (C_{l_β}).

This is one of the most complex derivatives to quantify since is numerically small and has many identifiable contributions. In this study, the contributions related to the interactions wing-fuselage and fin-fuselage are not taken into account. On the other hand dihedral (Γ) is considered to have the most significant contribution. By definition roll moment (L_R) is given by:

$$L_R = L_{R_{right}} + L_{R_{left}} = -\rho V \int_0^{b/2} c_y a_y \Gamma y dy \tag{19}$$

where c_y is the local chord and a_y is the local lift curve slope. In order to have a stable aircraft, a negative rolling moment is needed in order to restore the aircraft to level condition as shown in the lower part of Figure 9. The comparison of the results point to some expected trends such as for all cases: (1) a stable rolling moment is observed, i.e. $C_{l_\beta} < 0$ and, (2) reduction in $\Delta V_v < 0$ leads to a reduction in C_{l_β}. However, comparing the individual designs, it can be seen that Model 1 produces less C_{l_β} than the baseline case (a reduction between 13% to 21%) and Model 2 has a difference in C_{l_β} that varies between 12% and 27% compared to the baseline case.

Now let us consider the yawing moment due to sideslip derivative C_{n_β}, also known as *weathercock* stability, which effectively provides an insight into an aircraft's the tendency to turn into the wind in the presence of a sideslip disturbance. This derivative can be estimated as follows:

$$C_{n_\beta} = \frac{N_{\beta_{fin}}}{1/2\rho V S b} = V_v C_{L_{\alpha_{fin}}} \tag{20}$$

where a positive value indicates that it is stabilizing as shown in the upper section of Figure 9. A comparison of this derivative for the different designs shows that compared to the baseline wing design, C_{n_β} for Model 1 decreased between 19% and 23%. The difference between Model 2 and the baseline design is less than 1%.

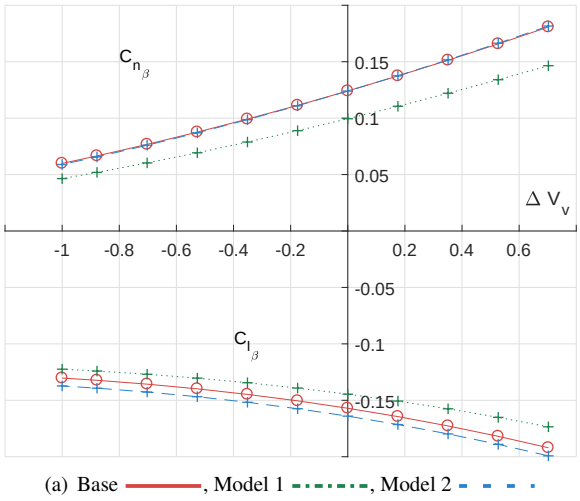

Figure 9 Rolling moment (C_{l_β}) and Yawing moment (C_{n_β}) due to sideslip

The aileron related roll and yaw derivatives (C_{l_ξ} and C_{n_ξ} respectively) provide some indication of the aircraft's tendency for adverse yaw. Starting with C_{l_ξ}, it can be estimated as follows:

$$C_{l_\xi} = \frac{L_\xi}{1/2\rho V^2 S b} = -\frac{1}{Ss} a_{2_A} \int_{y1}^{y2} c_y y dy \tag{21}$$

where $C_{L_{\alpha_{aileron}}}$ is the aileron lift slope and is considered constant along the aileron span. From the results presented in Figure 10(a) it can be observed that Model 1 presents a decrease of 49% in comparison to both the baseline case and Model 2 because the aileron used in this configuration is the same as the baseline case in terms of its spanwise position. As expected, Model 2 has the same behaviour as the baseline case because aileron characteristics are the same.

As for C_{n_ξ} this derivative can be estimated as follows:

$$C_{n\xi} = \frac{N_\xi}{1/2\rho V^2 Sb} = -\frac{1}{Ss}\int_{y1}^{y2}\left(\frac{\partial C_{D_y}}{\partial \xi}\right) c_y y dy \tag{22}$$

where for this equation is depended on C_D at the aileron strip (C_{D_y}). The results presented in Figure 10(b) show that Model 1 presents a difference that ranges from 88% to 102% when compared to the baseline and it even gives adverse yaw. Model 2 shows an increase with respect to baseline cases that ranges from 24% to 104% which is mainly driven by the higher C_{D_y} associated to the implemented twist distribution.

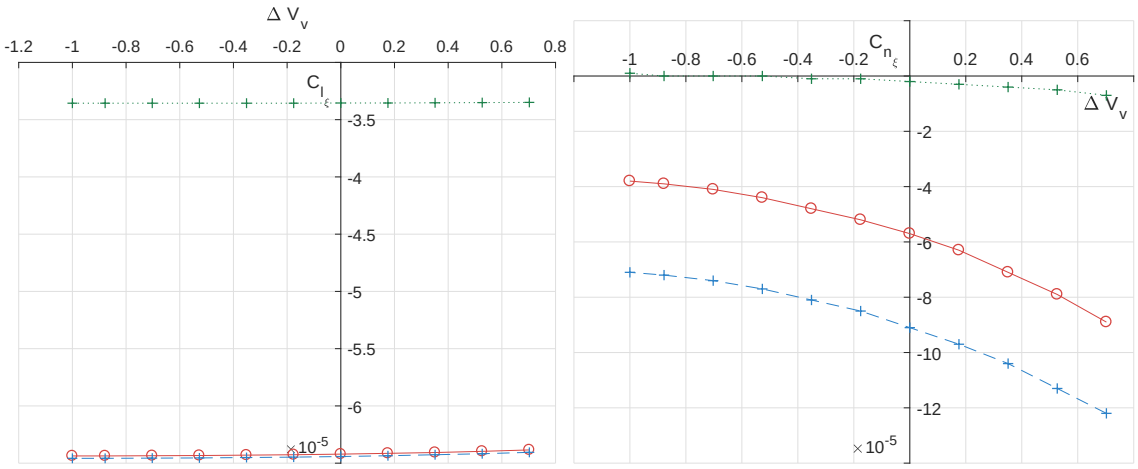

(a) Rolling moment due to Aileron C_{l_ξ} (b) Yawing moment due to Aileron C_{n_ξ}

Figure 10 Base ——, Model 1 -·-·-·-, Model 2 - - - -

B. Approach condition

Now that the characteristics for the cruise condition has been explored, the next step is to look into the approach phase. In this phase the stability and control characteristics are the more critical than aerodynamic performance. As in cruise condition, it is possible to see in Figure 11(a) that all three wing design cases have stable phugoid and short period modes. As for lateral-directional stability, inspection of Figure 11(b) shows that both the roll subsidence and spiral modes are also stable for all cases. However, considering the the Dutch roll mode it can be seen that the baseline design is only stable when $\Delta V_v = -0.52$. Model 1 is stable up to $\Delta V_v = -0.7$ and Model 2 has the same characteristics as Model 1.

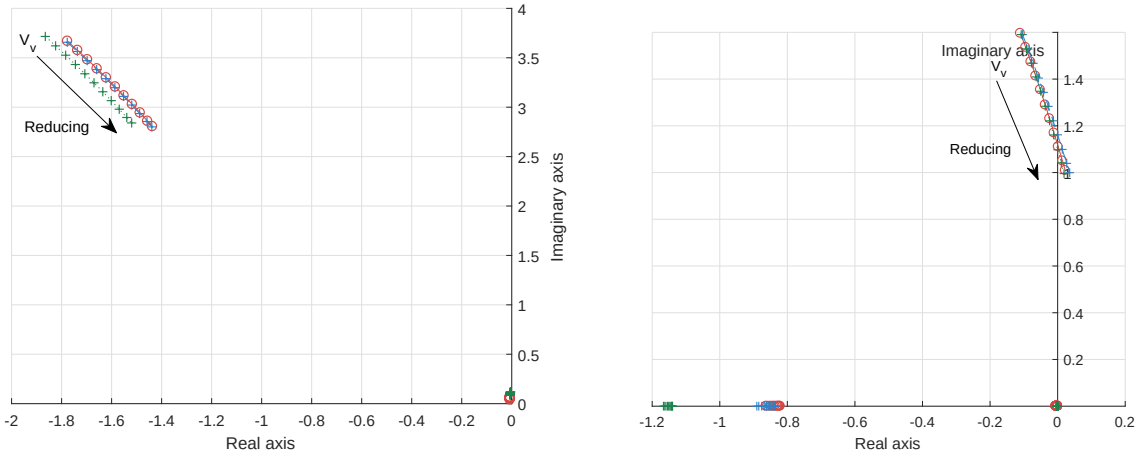

(a) Longitudinal stability root locus (b) Lateral stability root locus

Figure 11 Base ——, Model 1 -·-·-·-, Model 2 - - - -

Regarding the derivatives and starting with C_{m_α}, Figure 12(a) shows that it is not affected by the change in altitude and velocity and the magnitudes are similar to that in cruise. The same behaviour was found for C_{l_β} and C_{n_β} as can be seen in Figure 12(b). This is primarily due to the fact that this aircraft is designed for low subsonic cruise.

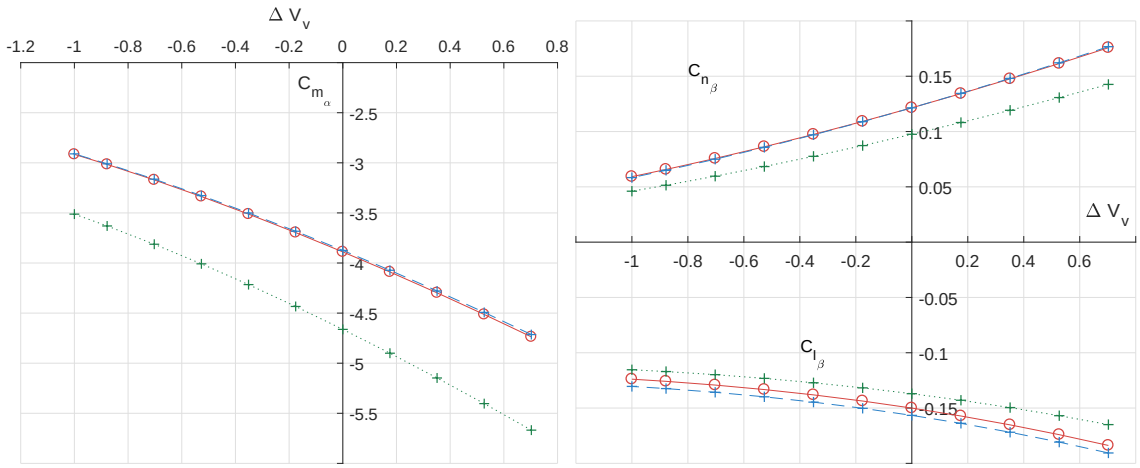

(a) C_{m_α} (b) C_{l_β} and C_{n_β}

Figure 12 Base ——, Model 1 -·-·-·-, Model 2 - - - -

Finally in the derivatives related to aileron deflection are shown in Figure 13(a). These show that there is no substantial change in C_{l_ξ}. However, for C_{n_ξ} the results in Figure 13(b) show that Model 1 still has a significant reduction in yawing moment due to aileron deflection in comparison to the baseline cases.

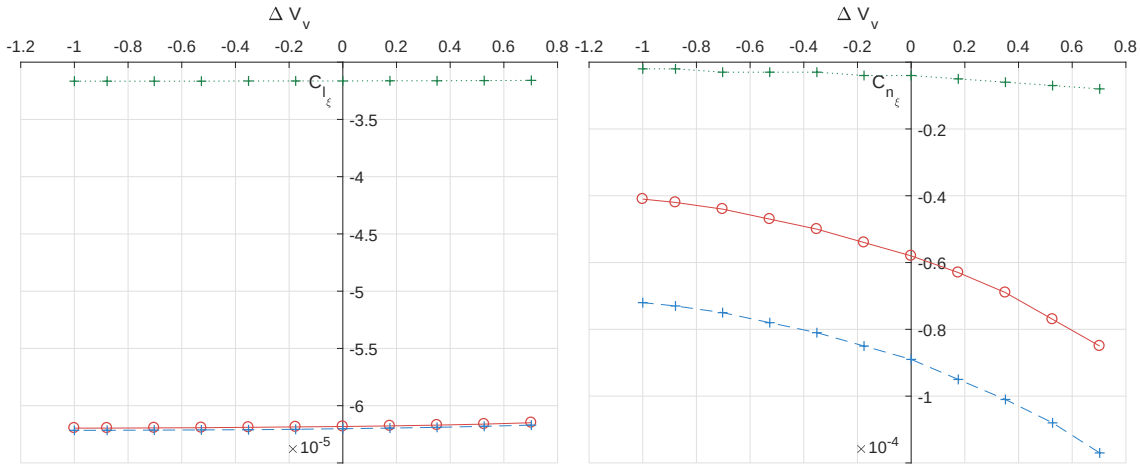

(a) Rolling moment due to Aileron C_{l_ξ} (b) Yawing moment due to Aileron C_{n_ξ}

Figure 13 Base ——, Model 1 -·-·-·-, Model 2 - - - -

VI. Conclusions and future work

In this study, the authors look into a way to reduce the weight of the aircraft by modifying the wing using an approach proposed by Prandtl in 1933 which advocated the use of a non-elliptic lift distribution combined with span extension to give improved performance. Moreover, such a distribution has also been found suitable for addressing the adverse yaw characteristics seen on flying wings. Here, the authors carry out a parameter variation study where the size of the vertical tailplane is reduced systematically for a general aviation aircraft to reduce its airframe weight and thus improve its range. This parameter variation study is carried out for three design cases which consist of a baseline design, a wing with only twist modifications (Model 2) and finally, a wing which adheres fully to Prandtl's 1933 method (Model 1). An aerodynamic

performance analysis and flight stability and control assessment is carried out for cruise flight conditions and the approach phase is also considered. In terms of aerodynamic performance it was found that Model 1 could deliver improvements in aerodynamic efficiency due to the increase of C_L while maintaining the same C_D values that the baseline configuration. Model 1 was found to increase the theoretical range of the aircraft by 7% to 17%. However, it was also noticed that if the ailerons are not correctly sized and positioned for such a design configuration, aileron effectiveness is compromised. It was also found that modifying the twist distribution for a wing designed to exhibit the classical elliptic lift distribution (Model 2) only yields an increase in rolling moment due to sideslip and the yawing moment due to aileron deflection when compared to the baseline model. As expected both Model 1 and Model 2 present a destabilising Dutch roll mode at cruise conditions for cases where the VTP size was reduced. Given the above conclusions it is necessary to look into finding the correct sizing of the aileron in Model 1 to have a similar $C_{l\xi}$ and $C_{n\xi}$ behaviour as the one for the baseline configuration. Moreover, this has been a simple parameter variation study and the authors intend to perform a multi-objective optimization study in order to explore the design tradeoffs between performance, stability, and airframe weight with the aim to explore the potential of the method proposed by Prandtl in 1933.

Acknowledgments

The authors wish to thank CONACYT, I^2T^2 and Cranfield University for supporting this research.

References

[1] Obert, E., *Aerodynamic design of transport aircraft*, IOS Press, 2009.
[2] Piquet, B. and Blumendeld, L., "A350XWB Special Edition," *Airbus Technical Magazine*, , No. June, jun 2013, pp. 25.
[3] Hale, J., "Boeing 787 from the Ground Up," *AERO QTR_4.06*, 2006, pp. 9.
[4] Raymer, D. P., *Aircraft Design (A Conceptual Approach)*, American Institute of Aeronautics & Astronautics, Washington D.C., 2nd ed., 1992.
[5] Van Dam, C., Holmes, B., and Pitts, C., "Effect of winglets on performance and handling qualities of general aviation aircraft," *Aircraft Systems Meeting*, American Institute of Aeronautics & Astronautics, Anaheim, CA, 1980, pp. 1–7.
[6] Prandtl, L., "Über Tragflügel kleinsten induzierten Widerstandes," *Zeitschrift für Flugtechnik und Motorluftschiffahrt*, Vol. 24, No. 11, 1933, pp. 305–306.
[7] Bowers, A. H., Murillo, O. J., Jensen, R. R., Eslinger, B., and Gelzer, C., "On Wings of the Minimum Induced Drag: Spanload Implications for Aircraft and Birds," Tech. Rep. March, NASA, Edwards, California, 2016.
[8] Drela, M. and Giles, M. B., "Viscous-inviscid analysis of transonic and low Reynolds number airfoils," *AIAA Journal*, Vol. 25, No. 10, oct 1987, pp. 1347–1355.
[9] Margason, R. J. and Lamar, J. E., "CHARACTERISTICS OF COMPLEX PLANFORMS," Tech. rep., Langley Research Center, Hampton, VA, 1971.
[10] Miranda, L. R., Elliott, R. D., and Baker, W. M., "A Generalized Vortex Lattice Method for Subsonic and Supersonic Flow Applications," Tech. rep., National Aeronautics and Space Administration, Burbank, CA, 1972.
[11] Anderson Jr, J., *Fundamentals of Aerodynamics*, Vol. Third Edit, McGraw-Hill Education, 5th ed., 2011.
[12] Clancy, L. J., *Aerodynamics*, Wiley, New York, 1975.
[13] Kelbe, R. J., Hill, N. M., Ladeinde, T. A., and Venkatasubban, C. S., "Loads Certification of the Cirrus Aircraft SF50 Vision Jet ®," *55th AIAA Aerospace Sciences Meeting*, AIAA, Grapevine, TX, 2017, p. 7.
[14] FLARIS, "FLARIS LAR 01," 2018.
[15] Purser, P. E. and Campbell, J. P., "EXPERIMENTAL VERIFICATION OF A SIMPLIFIED VEE-TAIL THEORY AND ANALYSIS OF AVAILABLE DATA ON COMPLETE MODW WITH VEE TAILS," Tech. rep., National Advisory Committee for Aeronautics, Langley Field, VA, 1945.

2019-01-07

Non-elliptic lift distribution wings to decrease vertical tailplane size in commercial aircraft

Carrizales Rodriguez, Martin Alejandro

AIAA

Carrizales MA, Bragado Aldana E, Lone MM. (2019) Non-elliptic lift distribution wings to decrease vertical tailplane size in commercial aircraft. Proceedings of the AIAA Scitech 2019 Forum, 7-11 January, San Diego, CA, USA

https://doi.org/10.2514/6.2019-0265